Observations of Comet 19P/Borrelly by the Miniature Integrated Camera and Spectrometer Aboard Deep Space 1

L. A. Soderblom,[1]* T. L. Becker,[1] G. Bennett,[1] D. C. Boice,[2] D. T. Britt,[3] R. H. Brown,[4] B. J. Buratti,[5] C. Isbell,[1] B. Giese,[6] T. Hare,[1] M. D. Hicks,[5] E. Howington-Kraus,[1] R. L. Kirk,[1] M. Lee,[5] R. M. Nelson,[5] J. Oberst,[6] T. C. Owen,[7] M. D. Rayman,[5] B. R. Sandel,[4] S. A. Stern,[8] N. Thomas,[9] R. V. Yelle[4]

The nucleus of the Jupiter-family comet 19P/Borrelly was closely observed by the Miniature Integrated Camera and Spectrometer aboard the Deep Space 1 spacecraft on 22 September 2001. The 8-kilometer-long body is highly variegated on a scale of 200 meters, exhibiting large albedo variations (0.01 to 0.03) and complex geologic relationships. Short-wavelength infrared spectra (1.3 to 2.6 micrometers) show a slope toward the red and a hot, dry surface (≤345 kelvin, with no trace of water ice or hydrated minerals), consistent with ~10% or less of the surface actively sublimating. Borrelly's coma exhibits two types of dust features: fans and highly collimated jets. At encounter, the near-nucleus coma was dominated by a prominent dust jet that resolved into at least three smaller jets emanating from a broad basin in the middle of the nucleus. Because the major dust jet remained fixed in orientation, it is evidently aligned near the rotation axis of the nucleus.

Comets are thought to be frozen records of the ancient primordial material from which the planets formed 4500 million years ago. They delivered some of the inventory of water and organic material to early Earth that enabled life to emerge. Their importance in the origin and evolution of our solar system and their potential role in the biological world has moved them to high priority for close-up scientific examination. Enabled by modern technology, spacefaring nations now have a number of projects under way to send probes to explore and sample comets over the next decade.

Comets 1P/Halley and 19P/Borrelly are the only comets whose nuclei have been imaged close-up by spacecraft (*1*). Halley is an intermediate-period comet that is believed to be compositionally representative of distant long-period comets in the Oort cloud (*2*). By contrast, Borrelly is a member of the short-period Jupiter-family comets, which are believed to have formed in the Kuiper Belt (*2*). They constitute about 15% of known comets. Most comets appear to be surprisingly uniform in gas composition; they are rich in water and have lesser amounts of CO, CO_2, and other volatiles. However, relative to Halley and long-period comets, many of the Jupiter-family comets—including Borrelly—appear to be considerably depleted in carbon-chain molecules (C_2, C_3, and longer chain hydrocarbons) (*3*). This difference is thought to reflect compositionally distinct regions where comets formed. The Borrelly observations discussed here represent our first view of a Jupiter-family comet nucleus and substantially broaden our understanding of what comets are like.

The NASA-JPL Deep Space 1 mission (DS1) is the first ion-propulsion spacecraft ever flown in deep space (for mission details, see http://nmp.jpl.nasa.gov/ds1). Launched in October 1998, DS1 spent a year proving out a variety of advanced spacecraft technologies as part of NASA's New Millennium Program (*4*). Later, its focus was turned on the scientific exploration of Borrelly (*5*). On 22 September 2001, DS1 passed 2171 ± 10 km from the comet's nucleus on the sunward side at a relative speed of 16.5 km/s. Here, we describe scientific findings from the Miniature Integrated Camera and Spectrometer [MICAS (*6*–*8*)] that collected visible-wavelength images and short-wavelength infrared spectra.

Borrelly has an orbital period of 6.86 years, a perihelion distance of 1.358 astronomical units (AU), and an orbital inclination of 30.3° (*9, 10*). The DS1 flyby occurred only 8 days after Borrelly's perihelion passage. During the DS1 approach, the view of the comet was in the direction of ecliptic south as it rose in its inclined orbit toward the spacecraft (Fig. 1). During the last ~90 min before closest approach, when the nucleus and details of the coma and dust jets were resolved, 52 visible-wavelength images and 45 short-wavelength infrared spectra (1.3 to 2.6 μm) were collected with MICAS. The images cover solar phase angles from 88° to 52° and provide stereoscopic coverage of the coma, jets, and nucleus. For all images of the comet shown in this article, the sunlight comes from the left of the frame.

Nucleus topography and morphology. We have determined the size and shape and mapped the morphological surface features of the nucleus of Borrelly from high-resolution images (47 to 58 m/pixel) (Figs. 1 to 3). The elongate nucleus is 8 km long, in good agreement with the Hubble Space Telescope estimate (*11*). The Borrelly nucleus is highly variegated in its terrains and morphological features. The nucleus can be divided into two terrain units: smooth and mottled terrain. No fresh impact craters down to ~200 m diameter are evident, which indicates a young and active surface. A number of rounded depressions are visible, but it is difficult to unambiguously identify any of them as impact craters. Images of this quality and scale acquired of any minor satellite or asteroid to date show ample impact craters. Rounded depressions are most abundant in the mottled terrain, but these all have similar diameters,

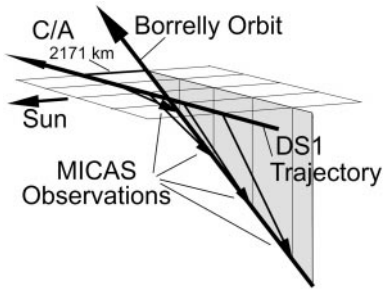

Fig. 1. Flyby geometry. Highest resolution images were acquired during the last 10,000 km (or about 10 min) before closest approach (C/A) as Borrelly rose in its inclined orbit toward the spacecraft. The DS1 trajectory was nearly in the plane of the ecliptic.

[1]United States Geological Survey, 2255 North Gemini Drive, Flagstaff, AZ 86001, USA. [2]Southwest Research Institute, 6220 Culebra Road, San Antonio, TX 78238, USA. [3]Department of Geological Sciences, University of Tennessee, 306 Geological Sciences Building, Knoxville, TN 37996, USA. [4]Department of Planetary Science, Lunar and Planetary Laboratory, University of Arizona, Tucson, AZ 85721, USA. [5]Jet Propulsion Laboratory (JPL), California Institute of Technology, 4800 Oak Grove Drive, Pasadena, CA 91109, USA. [6]DLR Institute of Space Sensor Technology and Planetary Exploration, Rutherfordstrasse, 2D-12489 Berlin, Germany. [7]Institute for Astronomy, University of Hawaii, 2680 Woodlawn Drive, Honolulu, HI 96822, USA. [8]Department of Space Studies, Southwest Research Institute, 1050 Walnut Street No. 426, Boulder, CO 80302, USA. [9]Max-Planck-Institut für Aeronomie, Max-Planck-Strasse 2, 37191 Katlenburg-Lindau, Germany.

*To whom correspondence should be addressed. E-mail: lsoderblom@usgs.gov

indicating that they may be the product of surface desiccation and collapse.

The smooth terrain occupies the broad basin that dominates the central part of the comet and is found on the small sunward end of the elongate nucleus (Figs. 4 and 5). Relative to the mottled terrain, the smooth terrain shows a higher average albedo (~0.03) and is smoother than average at the 50-m resolution limit. Several mesa-like features, which may be associated with the active jets, are within this terrain unit.

The mottled terrain, which consists of areas that are rough at ~200 m scale, exhibits irregular pits, bumps, troughs, and ridges. The textures could arise as ice sublimates, leaving piles of rubble. This unit is generally darker than average, shows strong albedo variation, and appears to be largely inactive (not associated with sources of gas and dust). The mottled terrain may represent older surface lag.

Within the mottled terrain at the larger end of the elongate object, there are streaks that radiate from the boundary with the smooth terrain. These may be structural in nature or may represent overlaying mantles caused by the transport of dust by the jets. In the narrowest part of the comet, a complex set of subparallel ridges and fractures is oriented normal to the long axis of the comet. The small end of the comet (that part beyond the necked-down, densely fractured corridor) is canted about 15° to 20° relative to the flat region containing the smooth terrain. Perhaps Borrelly's nucleus has been subject to complex compressional and/or extensional stresses that were produced during the comet's orbit or by gravitational interactions with planets, principally Jupiter. Alternatively, the fracturing could date from Borrelly's early collisional history in the Kuiper Belt (*12*). Conceivably, the shape of and structures in the nucleus are proof of its formation by coalescence of multiple bodies (*13*).

Photometry and spectroscopy of the nucleus. DS1 MICAS charge-coupled device (CCD) images show that the surface of Borrelly's nucleus is covered by dark material having an average geometric albedo of only 0.03 ± 0.005, with darker spots ranging down to ~0.01. The disk-integrated solar phase curve (Fig. 6) was generated from a combination of DS1 images (solar phase angle 52° to 88°) and published estimates for the bare nucleus at smaller solar phase angles (*11, 14*). The intensity of the coma was subtracted from each DS1 image. The phase curve is very similar to that of the dark C-type asteroid 253 Mathilde encountered by the NEAR spacecraft in 1997 (*15, 16*).

Several of the darkest spots on the nucleus

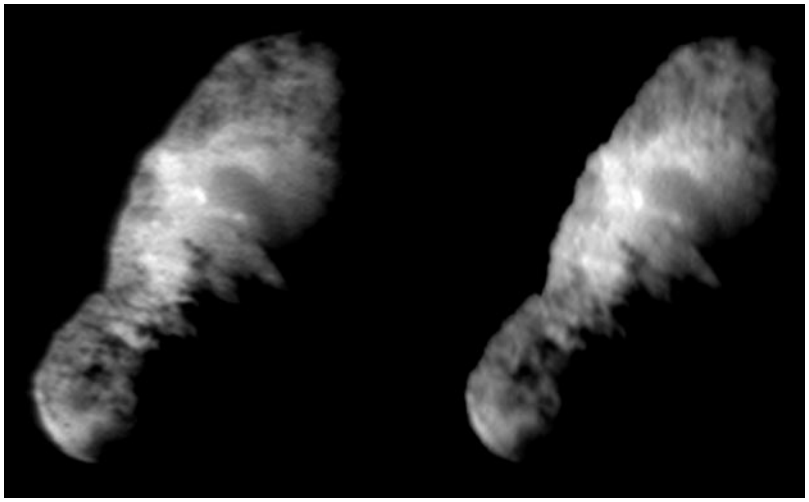

Fig. 3. Highest resolution stereo pair. Although the convergence angle between the two is only 4.4°, this pair best shows the smallest detail visible on the nucleus (ranges 3960 and 3560 km with resolutions of 52 and 47 m/pixel and phase angles of 56.0° and 51.6°).

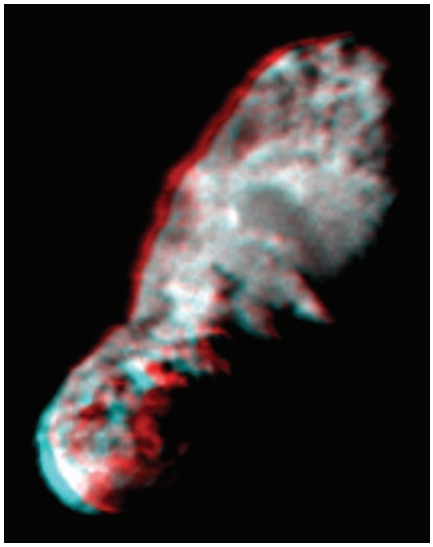

Fig. 2. Nucleus anaglyph made from two images with a convergence angle of 8°, acquired at ranges of 4390 and 3560 km with resolutions of 58 and 47 m/pixel and phase angles of 59.6° and 51.6° (view with standard red-blue anaglyphic glasses).

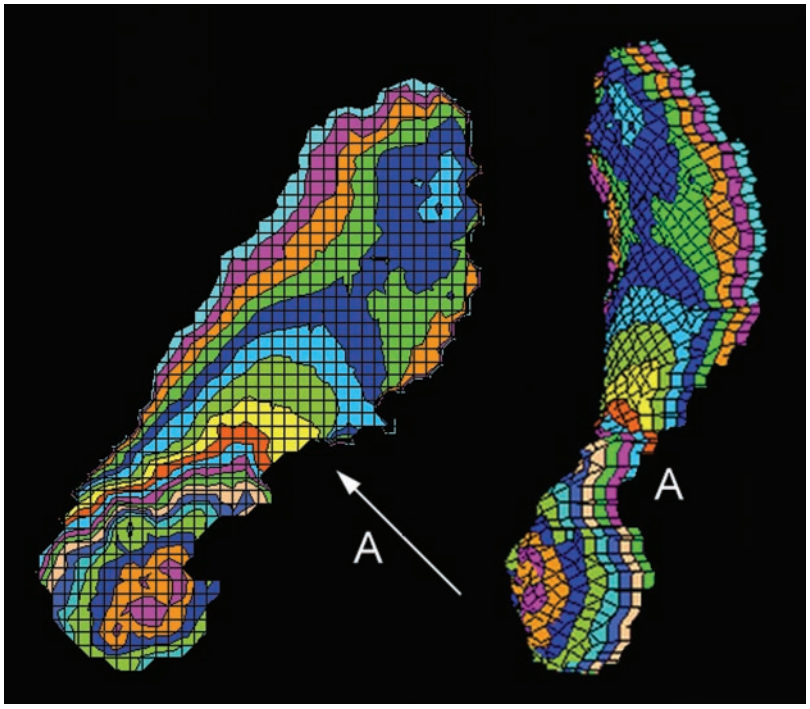

Fig. 4. Three-dimensional model of Borrelly's nucleus made from stereogrammetric analysis. Left: Map of range from the spacecraft to the surface for the highest resolution image (left image in Fig. 3). Right: Perspective view A has been rotated into the direction shown by arrow A, elevated 45° out-of-plane. Colors: 200-m range contours.

represent true albedo variations rather than simply being due to shadowing. Dark spots just inside the terminator show a very weak change with phase, characteristic of the coma. The dark spots centered in the illuminated small end of the nucleus, however, vary in brightness with solar phase angle in the same way as adjacent brighter areas. Our topographic model indicates that these spots are ~45° from the subsolar point. We conclude that the range of albedo from darkest spots to brightest patches is about a factor of 3 and the albedo ranges from ~0.01 to ~0.035. The darkest albedo spots could be compositionally different materials or may have different particle size and compaction effects.

The generally accepted value for the albedo of cometary nuclei that is used in most comet studies is ~0.04, although lower estimates have been reported (*17, 18*). Our range of low albedo for Borrelly was validated through calibration with MICAS observations of Mars and Jupiter. These lower albedos are comparable to those of a number of objects in the outer solar system, including several C-type asteroids (0.02 to 0.03) (*19*), the rings of Uranus (~0.03) (*20*), and the dark side of Saturn's moon Iapetus, which ranges down to ~0.01 (*21*).

The MICAS instrument includes a short-wavelength infrared imaging spectrometer (SWIR) that operates from 1.3 to 2.6 μm and collects 0.007-μm spectral samples (*6*). This channel maps a target with 256 fields of view (54 μrad each) arranged along the spectrometer slit. Just before closest approach (–157 s, range 2910 km, phase angle 41°), a long-exposure observation (28 s) was initiated with the hope of capturing the nucleus in the SWIR channel by sweeping the slit across the best predicted position for the nucleus. This yielded SWIR spectra for 45 swaths across the nucleus. Each swath was oriented with its long axis across the short dimension of the nucleus in the sunward direction and with its width of ~165 m along the length of the nucleus (Fig. 7).

The nucleus reflectance spectrum has a strong slope toward the red. A single absorption feature is consistently visible in all 45 spectra at ~2.39 μm and is ~0.02 μm wide. The origin of the absorption feature is not known; however, various hydrocarbons such as polyoxymethylene (*22–24*), suggested as compositional candidates for cometary nuclei, exhibit absorption features in this region.

At Borrelly's distance from the Sun at the time of the encounter, the equilibrium temperature of a nonrotating body with an albedo of 0.03 and an emissivity of 0.9 would be ~345 K. Even though the peak emission for this temperature is near 8 μm, the blue end of the Planck function extends well into the MICAS spectral range between 2 and 2.5 μm, allowing temperature fits to the spectral swaths across the nucleus (Fig. 7). The high temperatures, which range continuously from 300 to 345 K, are consistent with the lack of any trace of H_2O ice bands (or hydrated minerals) in the spectra. The lack of water ice is also consistent with the strong slope toward the red. Many solar system objects that are reddish in visible wavelengths do not show strong red slopes in the SWIR because of the presence of water (*24*). The lack of water ice and the high average temperatures are also consistent with estimates that only ~10% or less of the nucleus surface is actively sublimating to generate the observed OH production rate (a photodissociation product of water) and dust concentration (*11*). We note that because the footprint of each spectrum is a swath running from the Sun-facing limb to the opposite terminator, the hot dry regions dominate the spectrum, and cold regions expected for actively sublimating ice (~200 K) will be masked.

Near-nucleus coma and dust jets. Borrelly has historically exhibited a strong sunward asymmetry in its coma over the ~100 years and 13 apparitions in which it has been observed. This manifests itself as an elongation of the coma toward the Sun. In contrast with the view from Earth, the DS1 view during approach was downward toward the ecliptic south pole as the comet rose in its inclined orbit toward the spacecraft (Fig. 1). During approach, the sunward asymmetry of the coma was resolved to a narrow dust beam only a few kilometers in width at its base where it emanated from the broad central basin on the nucleus (Fig. 8). This jet-like dust feature, which we call the α jet, was canted about 30° from the direct Sun line. In the DS1 images, it extends out to a range of ~100 km, where its brightness falls below the detection limit in the images ($\sim 10^{-6}$ the brightness of a 100% reflecting surface).

High-resolution views show that the main features in Borrelly's near-nucleus coma fall into two classes—collimated jets and fans—

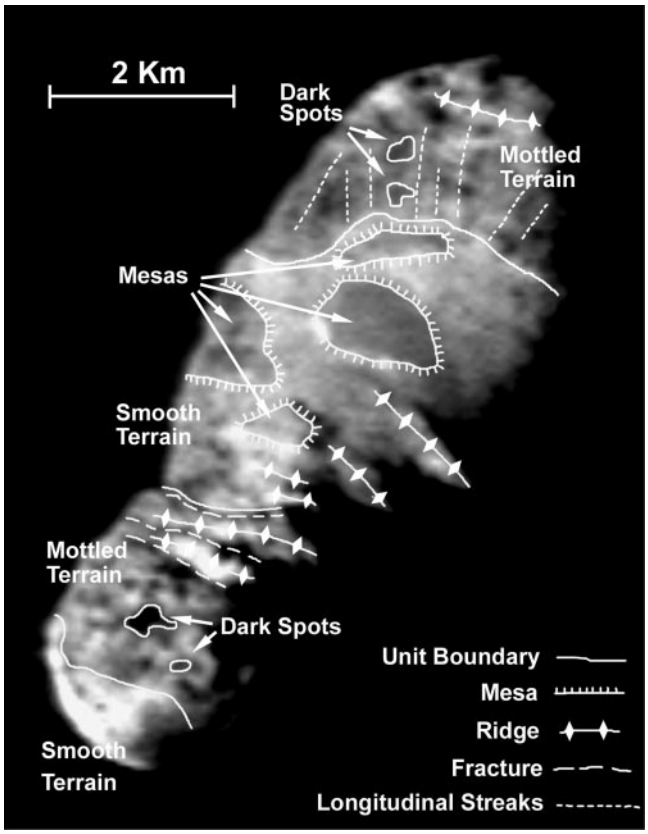

Fig. 5. Sketch map of morphological units and features.

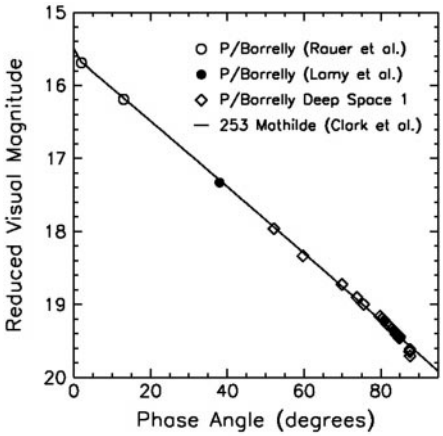

Fig. 6. Disk-integrated solar phase curve for Borrelly's nucleus. DS1 MICAS observations have been combined with Earth-based observations by Lamy *et al.* (*11*) and Rauer *et al.* (*14*) and fitted with the phase dependence observed for Mathilde. Visual magnitudes have been reduced to a range of 1 AU for both Sun and observer.

also observed at Halley (*1, 25*). By creating a movie of the seven best images, we have been able to discern and separate two sets of collimated dust jets. The α jet (Fig. 8A) is aligned at the core of the main jet seen for several weeks during the approach. The β jet is one of several roughly parallel smaller collimated jets contained in the main jet but offset in the images ~15° from the direction of the α jet (Fig. 8B). The fan-shaped feature, second in brightness only to the main jet, is seen in both images and is centered on the Sun line originating from a spatially extended source across the small, smooth end of the nucleus.

Each collimated jet has a cylindrical core, 200 to 400 m in radius and 4 to 6 km in length, with a typical spacing of ~1 km between jets. Bright hemispheric-shaped isophotes are visible at the bases of the β jets, particularly when they are well resolved and their sources are near the limb. Two of the β jets are traceable to surface sources that appear as dark (possibly depressed) patches in or adjacent to the bright smooth terrain. This simple extrapolation may, however, not be appropriate in this complex region of dusty gas flow.

Whereas the dust fan is centered roughly on the Sun line, the collimated jets have sufficiently discrete directions that their three-dimensional orientations can be determined. The angle of each jet was measured relative to the image field of view. These angles changed as the spacecraft turned and rotated as it flew past the comet. From best fit solutions, the α jet (the core of the main jet) is estimated to have been ~30° forward of the Sun line (prograde sense) and about 10° above the ecliptic (right ascension 218.5° ± 3°, declination −12.5° ± 3°). The best imaged β jet (Fig. 8B) was offset from the α jet by ~35° (right ascension 240° ± 5°, declination 15° ± 5°).

A model of dust carried from the nucleus by radially expanding gas would have a dust abundance that would fall off as $1/r^2$, where r is the distance from the source (so long as the dust properties, for example particle size, are unchanging). In projection, this would produce a $1/r$ falloff in brightness in the image. Diffuse regions of the near-nucleus coma (the fan radiating from the Sun-facing end and gaps between collimated jets and regions of the coma extending toward the night side) all exhibit this characteristic $1/r$ profile.

By contrast, the highly collimated jets exhibit a much slower falloff in brightness than $1/r$ out to a range of ~ 5 km; the β jet (Fig. 8B) departed markedly from a simple $1/r$ behavior. This jet retains roughly constant brightness out to ~5 km, after which it falls off in the conventional $1/r$ behavior. Various workers have considered fragmentation of coarse particles in modeling dust-gas interaction in cometary jets (*26*). We interpret the behavior of the narrow collimated jets to indicate that they contain relatively coarse (on the order of 10 μm) icy dust particles that, once accelerated, travel ballistically in a narrow beam, undeflected by expanding gas. These particles soon fragment by sublimation. The time of flight through the visible core of the α jet is probably on the order of 10 s (assuming a typical gas-dust speed of 0.4 km s^{-1}). We estimate that the sublimation lifetime of a 10-μm particle is roughly the same, depending on the ice/dust mass fraction. In this picture, the coarse particles sublimate and fragment, dispersing into a cloud of very fine dust particles.

Borrelly's main jet was observed for several weeks before encounter. Images acquired 11 and 34 hours before encounter have sufficiently high resolution to show the direction of the main jet to be within ±5° of that observed at encounter. The main jet was thus observed to be stationary for longer than the observed nucleus rotation period of 26 hours (*27*). We conclude that the main jet is nearly aligned with the rotation axis of the nucleus. This places the subsolar latitude at ~60°N latitude and the pole in constant sunlight during perihelion passage. This direction for the pole is consistent with the stable rotation of the nucleus around its short axis. Nongravitational forces arising from the nearly on-axis main jet would have a minimal effect on this stable rotational state.

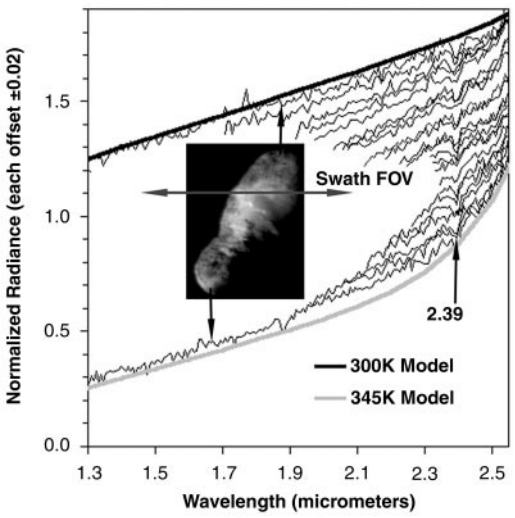

Fig. 7. Short-wavelength infrared spectra of the nucleus, showing a 2.39-μm absorption feature. Spectra are normalized at 2.359 μm and are incrementally offset from one another by 0.02. The central void results from instrument saturation. Curves are model temperature fits at two ends. Coma is negligible in these spectra.

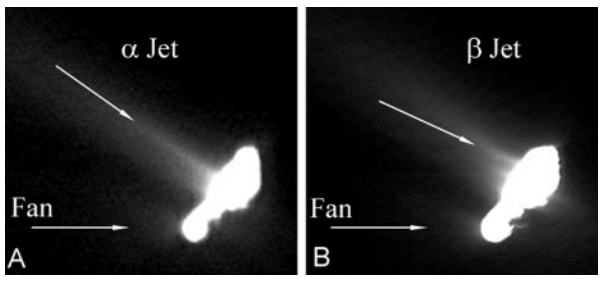

Fig. 8. Near-nucleus coma and dust features: (**A**) Range ~13,130 km, resolution 173 m/pixel, phase angle ~79.6°. (**B**) Range ~4825 km, resolution 63 m/pixel, phase angle ~62.5°.

References and Notes

1. H. U. Keller *et al.*, *Astron. Astrophys.* **187**, 807 (1987).
2. Comets are grouped into dynamical classes according to their orbital characteristics. According to (*28*), known comets now include 211 short-period (SP) comets (also known as Jupiter-family) with periods less than about 30 years, 37 intermediate-period (IP) comets (also known as Halley-family) with periods of about 30 to 200 years, and 1166 long-period (LP) comets with periods >200 years. The source region of the SP comets is thought to be the Kuiper Belt, a torus-shaped region just beyond the orbit of Neptune, where they formed. LP comets come from the Oort cloud, a roughly spherical distribution of comets at the extreme limits of our solar system (a few tens of thousands of AU from the Sun). It is generally believed that Oort cloud comets originated in the Uranus-Neptune region and were then gravitationally scattered into the Oort cloud, whereas IP comets formed in the same region but were scattered into the region of the Kuiper Belt.
3. M. F. A'Hearn *et al.*, *Icarus* **118**, 223 (1995).
4. M. D. Rayman *et al.*, *Acta Astron.* **47**, 475 (2001).
5. M. D. Rayman, P. Varghese, *Acta Astron.* **48**, 693 (2001).
6. MICAS is a four-channel instrument that integrates two visible-wavelength cameras [CCD and active pixel sensor (APS)] and two imaging spectrometers (ultraviolet and SWIR). The ultraviolet imaging spectrometer detector failed soon after launch, and the APS camera was set up for bright targets. Therefore, the Borrelly observations were acquired with the CCD camera (1024 × 1024 array; image field of view, 13.14 mrad; spectral bandpass, 0.5 to 1.0 μm full width at half maximum) and the SWIR (Rockwell NICMOS-3 PICNIC detector array; spectral range, 1.3 to 2.6 μm; spectral sampling of 7 μm). MICAS was modeled after the Planetary Integrated Camera and Spectrometer (PICS). Radiometric units used in this article are I/F, where I is the intensity and πF is the incident solar flux at the comet's range from the Sun, both integrated over the instrument spectral re-

sponse. A perfectly reflecting, white Lambertian disk would have an *I/F* of 1.0.
7. P. M. Beauchamp *et al.*, in *Proceedings of the 8th Annual AIAA/ Utah State University Conference on Small Satellites*, Logan, UT, 29 August to 1 September 1994.
8. L. A. Soderblom *et al.*, in *Proceedings of the DS1 Technology Validation Symposium*, Pasadena, CA, 8 to 9 February 2000.
9. *IAU Minor Planet Circular 31664* (1998).
10. Comet 19P/Borrelly was discovered on 28 December 1904 by Alphonse Louis Nicolas Borrelly of Marseilles, France.
11. P. L. Lamy *et al.*, *Astron. Astrophys.* **337**, 945 (1998).
12. P. Farinella, D. R. Davis, S. A. Stern, in *Protostars and Planets IV*, V. Mannings, A. P. Boss, S. S. Russell, Eds. (Univ. of Arizona Press, Tucson, AZ, 2000), p. 1255.
13. P. R. Weissman, *Nature* **320**, 242 (1986).
14. H. Rauer *et al.*, *Bull. Am. Astron. Soc.* **31**, 1131 (1999).
15. J. Veverka *et al.*, *Science* **278**, 2109 (1997).
16. B. Clark *et al.*, *Icarus* **140**, 53 (1999).
17. M. S. Hanner *et al.*, *Icarus* **62**, 97 (1985).
18. G. J. Veeder *et al.*, *Astron. J.* **94**, 169 (1987).
19. E. Tedesco *et al.*, *Astron. J.* **97**, 580 (1989).
20. M. E. Ockert *et al.*, *J. Geophys. Res.* **92**, 14969 (1987).
21. B. J. Buratti, J. A. Mosher, *Icarus* **115**, 219 (1995).
22. W. F. Huebner, *Science* **237**, 628 (1987).
23. D. L. Mitchell *et al.*, *Science* **237**, 626 (1987).
24. D. P. Cruikshank *et al.*, *Icarus* **135**, 389 (1988).
25. J. Knollenberg *et al.*, *Earth Moon Planets* **72**, 103 (1996).
26. I. Konno *et al.*, *Icarus* **116**, 77 (1995).
27. B. Mueller, N. Samarasinha, *Bull. Am. Astron. Soc.* **33**, 1090 (2001).
28. B. G. Marsden, *IAU Circular 7771* (2001).

3 January 2002; accepted 26 March 2002
Published online 4 April 2002;
10.1126/science.1069527
Include this information when citing this paper.

The *E. coli* BtuCD Structure: A Framework for ABC Transporter Architecture and Mechanism

Kaspar P. Locher,* Allen T. Lee, Douglas C. Rees*

The ABC transporters are ubiquitous membrane proteins that couple adenosine triphosphate (ATP) hydrolysis to the translocation of diverse substrates across cell membranes. Clinically relevant examples are associated with cystic fibrosis and with multidrug resistance of pathogenic bacteria and cancer cells. Here, we report the crystal structure at 3.2 angstrom resolution of the *Escherichia coli* BtuCD protein, an ABC transporter mediating vitamin B_{12} uptake. The two ATP-binding cassettes (BtuD) are in close contact with each other, as are the two membrane-spanning subunits (BtuC); this arrangement is distinct from that observed for the *E. coli* lipid flippase MsbA. The BtuC subunits provide 20 transmembrane helices grouped around a translocation pathway that is closed to the cytoplasm by a gate region whereas the dimer arrangement of the BtuD subunits resembles the ATP-bound form of the Rad50 DNA repair enzyme. A prominent cytoplasmic loop of BtuC forms the contact region with the ATP-binding cassette and appears to represent a conserved motif among the ABC transporters.

Since its discovery over a decade ago, the family of ABC transporter proteins has grown dramatically to well over a thousand examples with known sequences. ABC transporters now form the largest family of membrane-spanning transport proteins, ubiquitous in all branches of life (*1*). They invariably consist of two membrane-spanning domains that harbor a translocation pathway for a specific substrate, and two attached, water-exposed, and well-conserved ATP-binding cassettes (hence ABC) that power the transport reaction through hydrolysis of ATP (*2*, *3*). Several mammalian ABC transporters are medically relevant. For example, mutations in the cystic fibrosis transmembrane conductance regulator (CFTR) cause a dysfunction of this protein that represents the molecular basis of cystic fibrosis (*4*). A separate subclass of ABC transporters are related to multidrug resistance, exemplified by the human MDR1 and MRP1 proteins, whose overexpression in tumor cells causes resistance to various cytotoxic agents used in chemotherapy (*5*). Another clinically relevant ABC transporter is the TAP protein, which translocates antigenic polypeptides from the cytoplasm into the endoplasmic reticulum, where they are being loaded onto major histocompatibility complex (MHC) class I molecules (*6*, *7*). In bacteria, ABC transporters are predominantly involved in nutrient uptake, although they also participate in the export of bacterial toxins or harmful substances, contributing to bacterial multidrug resistance (*8*, *9*). Bacterial ABC transporters are generally assembled from up to four separate protein subunits, whereas their eukaryotic counterparts are generally composed of a single polypeptide.

A striking feature of the ABC transporter family is that it includes importers and exporters, and that the recognized substrates range from single chloride ions (in CFTR) to entire protein toxins (bacterial toxin exporters). This diversity of transported substrates is reflected in the poor sequence similarities of the membrane-spanning subunits and domains. What ties the family together are a number of highly conserved ABC cassette motifs (Fig. 1), many of which are directly involved in the binding and hydrolysis of ATP, such as the P loop or Walker-A motif, the Walker-B motif, a glutamine residue in the Q loop, and a histidine residue in the Switch region (*10*–*12*). In addition, ABC cassettes invariably possess a D loop (*13*) and a short polypeptide stretch (. . . LSGG . . .), which is so specific to this protein class that it is generally referred to as the "ABC signature sequence." In view of these similarities, it is generally assumed that all ABC cassettes bind and hydrolyze ATP in a similar fashion and use a common mechanism to power the translocation of substrate through the membrane-spanning partner domains.

The current view of the mechanism begins with binding of the substrate to the transporter. Importers in Gram-negative bacteria generally require a periplasmic binding protein that delivers the substrate to the periplasmic side of the transporter (*14*), whereas exporters recruit their substrates directly from the cytoplasm or, in the case of very hydrophobic substances, from the inner leaflet of the plasma membrane. The binding event is signaled to the nucleotide hydrolysis sites, where it is thought to increase the affinity for ATP, a prerequisite for a productive transport cycle. The two ABC cassettes then carry out the "power stroke," a highly cooperative ATP-binding and hydrolysis reaction that is concurrent with a substantial conformational change. This change is coupled to mechanistically critical rearrangements in the membrane-spanning domains associated with unidirectional substrate translocation, which is believed to occur through a tailored pathway at the domain interface. After the substrate has crossed the membrane, the transporter returns to the resting state through the dissociation of ADP and inorganic phosphate. As with other ATPases, orthovanadate inhibits ABC transporter function (*15*); for example, the bacterial maltose importer (MalFGM) was shown to be trapped close to the transition state, with ADP, ortho-vanadate, and the binding protein firmly associated, while the substrate (maltose) was already released (*16*). This suggests that during translocation, the maltose-binding protein may serve as a plug that prevents the substrate from escaping on the wrong side of the membrane. Similar experiments with the bacterial, drug-exporting LmrA

Howard Hughes Medical Institute and Division of Chemistry and Chemical Engineering, Mail Code 147-75CH, California Institute of Technology, Pasadena, CA 91125, USA.

*To whom correspondence should be addressed. E-mail: locher@caltech.edu, dcrees@caltech.edu